Published in final edited form as:
Eur J Neurosci. 2008 January ; 27(2): 352–363.

Characterization of GABAergic neurons in rapid-eye-movement sleep controlling regions of the brainstem reticular formation in GAD67–green fluorescent protein knock-in mice

Ritchie E. Brown[1,2], **James T. McKenna**[2], **Stuart Winston**[2], **Radhika Basheer**[2], **Yuchio Yanagawa**[3], **Mahesh M. Thakkar**[2,*], and **Robert W. McCarley**[2]

1*In Vitro Neurophysiology Section, Laboratory of Neuroscience, Harvard Medical School and VA Boston Healthcare System, 940 Belmont Street, Research 151-C, Brockton, MA 02301, USA*

2*Laboratory of Neuroscience, Harvard Medical School and VA Boston Healthcare System, Research 151-C, Brockton, MA, USA*

3*Department of Genetic and Behavioral Neuroscience, Gunma University Graduate School of Medicine and SORST, JST, Maebashi, Japan*

Abstract

Recent experiments suggest that brainstem GABAergic neurons may control rapid-eye-movement (REM) sleep. However, understanding their pharmacology/physiology has been hindered by difficulty in identification. Here we report that mice expressing green fluorescent protein (GFP) under the control of the GAD67 promoter (GAD67-GFP knock-in mice) exhibit numerous GFP-positive neurons in the central gray and reticular formation, allowing on-line identification *in vitro*. Small (10−15 μm) or medium-sized (15−25 μm) GFP-positive perikarya surrounded larger serotonergic, noradrenergic, cholinergic and reticular neurons, and >96% of neurons were double-labeled for GFP and GABA, confirming that GFP-positive neurons are GABAergic. Whole-cell recordings in brainstem regions important for promoting REM sleep [subcoeruleus (SubC) or pontine nucleus oralis (PnO) regions] revealed that GFP-positive neurons were spontaneously active at 3−12 Hz, fired tonically, and possessed a medium-sized depolarizing sag during hyperpolarizing steps. Many neurons also exhibited a small, low-threshold calcium spike. GFP-positive neurons were tested with pharmacological agents known to promote (carbachol) or inhibit (orexin A) REM sleep. SubC GFP-positive neurons were excited by the cholinergic agonist carbachol, whereas those in the PnO were either inhibited or excited. GFP-positive neurons in both areas were excited by orexins/hypocretins. These data are congruent with the hypothesis that carbachol-inhibited GABAergic PnO neurons project to, and inhibit, REM-on SubC reticular neurons during waking, whereas carbachol-excited SubC and PnO GABAergic neurons are involved in silencing locus coeruleus and dorsal raphe aminergic neurons during REM sleep. Orexinergic suppression of REM during waking is probably mediated in part via excitation of acetylcholine-inhibited GABAergic neurons.

Correspondence: Dr R. E. Brown, In Vitro Neurophysiology Section, as above. E-mail: Ritchie_Brown@hms.harvard.edu.
**Present address*: Department of Neurology, University of Missouri, Harry Truman Memorial VA Hospital, 800 Hospital Drive, Columbia, MO 65212, USA

Abbreviations CARB, carbachol; ChAT, choline acetyltransferase; –DC, hyperpolarizing direct current injection; +DC, depolarizing direct current injection; DAB, diaminobenzidine; DRN, dorsal raphe nucleus; GABA, γ-aminobutyric acid; GAD67, glutamate decarboxylase 67 kDa isoform; GFP, green fluorescent protein; I_h, hyperpolarization activated current; LC, locus coeruleus; LDT, laterodorsal tegmental nucleus; LPT, lateral pontine tegmentum; Mo5, motor trigeminal nucleus; MRN, median raphe nucleus; nNOS, neuronal nitric oxide synthase; Ox A, orexin A (hypocretin 1); PBS, phosphate-buffered saline; PnO, pontine nucleus oralis; PPT, pedunculopontine tegmental area; REM, rapid-eye-movement; SubC, subcoeruleus (alpha part + dorsal part); TrypH, tryptophan hydroxylase; TTX, tetrodotoxin; TyH, tyrosine hydroxylase; vlPAG, ventrolateral periaqueductal gray.

Keywords

carbachol; orexin; REM sleep; subcoeruleus; whole cell

Introduction

Recent experiments suggest that neurons utilizing the neurotransmitter γ-aminobutyric acid (GABA) are important in controlling the timing and amount of rapid-eye-movement (REM) sleep (Luppi *et al.*, 2004; McCarley, 2007). Injection of the $GABA_A$ receptor antagonists bicuculline or GABAzine into the subcoeruleus (SubC) or pontine nucleus oralis (PnO) regions of the reticular formation, where REM-on neurons are located, induces a REM-like state in rats and cats (Xi *et al.*, 1999; Boissard *et al.*, 2002; Pollock & Mistlberger, 2003; Sanford *et al.*, 2003). In contrast, infusion of $GABA_A$ receptor antagonists into the dorsal raphe nucleus (DRN) or locus coeruleus (LC), where REM-off serotonergic and noradrenergic neurons are located, abolishes the decrease in firing rate normally observed in these neurons during REM sleep (Gervasoni *et al.*, 1998, 2000). Measurements of GABA levels in freely behaving cats revealed that GABA levels increase in brainstem REM-off areas (DRN, LC) relative to values in slow-wave-sleep (Nitz & Siegel, 1997a, b), whereas they decrease in the pontine reticular formation (Thakkar *et al.*, 2004). Thus, at least two populations of GABAergic neurons probably exist, namely REM-on GABA neurons inhibiting aminergic neurons during REM sleep, and REM-off GABA neurons inhibiting REM-on reticular neurons during waking.

GABA is synthesized by the enzyme glutamate decarboxylase, which exists in two isoforms, GAD65 and GAD67. Although immunohistochemical and *in situ* hybridization studies suggest that both these isoforms are present in all GABA neurons (Esclapez *et al.*, 1993, 1994), gene knockouts indicate that GAD67 (encoded by the *Gad1* gene) is the major isoform involved in GABA synthesis (Asada *et al.*, 1996, 1997). Immunohistochemical studies utilizing staining for GAD67 coupled with c-Fos staining as a marker of neuronal activation have identified several populations of brainstem GABA neurons that may be involved in the control of REM sleep (Maloney *et al.*, 1999, 2000; Torterolo *et al.*, 2000, 2001; Boissard *et al.*, 2003; Lu *et al.*, 2006).

Combined injections of cholinergic and GABAergic agents suggest that GABA acts downstream of acetylcholine in the regulation of REM sleep (Xi *et al.*, 2004). One model to unify the role of acetycholine and GABA in the control of REM sleep would be acetycholine inhibition of GABAergic REM-off neurons, leading to disinhibition of REM-on effector neurons in the SubC/PnO. Thus, orexins (which are lost in the disease narcolepsy) would prevent REM sleep by exciting this same group of GABAergic neurons. In contrast, acetylcholine would excite REM-on GABA neurons. However, the electrical properties of GABAergic neurons and their response to neurotransmitters regulating behavioral state are unknown, largely due to difficulties in identification.

We thus used a novel mouse model in which green fluorescent protein (GFP) is expressed under control of the full promoter region of the *Gad1* gene (GAD67-GFP knock-in mice) (Tamamaki *et al.*, 2003). This investigation is, to our knowledge, the first to give a comprehensive picture of GABAergic neurons in the mesopons of the mouse and the first to test the effects of REM sleep neuromodulators on identified GABAergic brainstem neurons. Portions of this work have been presented in abstract form (Brown *et al.*, 2006a,b).

Materials and methods

Animals

The generation of GAD67-GFP (Δneo) mice has been described by Tamamaki *et al.* (2003), and these mice, used in the present study, were termed GAD67-GFP knock-in mice. GAD67-GFP knock-in mice were bred in-house at the animal facility of the Brockton Division of the VA Boston Healthcare system. These facilities are approved by the American Association for Accreditation of Laboratory Animal Care and are under full-time veterinary supervision. Mice were housed under constant temperature (23 °C) and a 12 h: 12 h light–dark cycle (lights-on period from 1:00 h to 22:00 h) with food and water available *ad libitum*. All animals were treated in accordance with the American Association for Accreditation of Laboratory Animal Care's policy on care and use of laboratory animals. The experiments described here were approved by the Institutional Animal Care and Use committee of the VA Boston Healthcare system (Protocol 172-B-0304). Phenotyping of mice was achieved by examining the heads of the mice 1−2 days after birth under a fluorescence microscope at ×4 magnification. Heterozygotic mice exhibited a striking green fluorescence in the brain and the olfactory bulb (visualized through the skull), as described in Tamamaki *et al.* (2003).

Immunohistochemistry

For immunohistochemistry, adult (3−12 months) heterozygous knock-in mice were deeply anesthetized with pentobarbital (50 mg/mL). For GABA immunohistochemistry, mice were perfused transcardially with 0.1% glutaraldehyde in 4% buffered paraformaldehyde (Sigma). For staining of other neuronal markers, the mice were perfused with just the 4% buffered paraformaldehyde solution. The brain was removed and placed in 30% sucrose. One day later, the brainstem was cut on a freezing microtome at 20 μm (GABA) or 40 μm (other stains) and stored in phosphate-buffered saline (PBS) at 4 °C until needed (1−5 days). Slices that contained areas of interest were washed three times in PBS for 10 min on a shaking platform at room temperature.

After the third wash, the slices were placed in a blocking solution (0.3% Triton X-100 in PBS containing 5% normal donkey serum) for 1 h. Slices were then incubated overnight at ambient temperature on a shaking platform with a solution containing the primary antibody in PBS with 0.3% Triton X-100 and 1% normal donkey serum. The following primary antibodies were used: rabbit polyclonal anti-GABA (Sigma, A2052, 1 : 5000 or 1 : 10 000); rabbit polyclonal anti-(tyrosine hydroxylase) (TyH) (Chemicon, AB5986, 1 : 500); sheep polyclonal anti-(tryptophan hydroxylase) (TrypH) (Chemicon, AB1541, 1 : 500); mouse monoclonal anti-(neuronal nitric oxide synthase) (nNOS) (Sigma, N2280, 1 : 400); rabbit anti-(choline acetyltransferase) (ChAT) (Chemicon, AB5042, 1 : 200); and mouse monoclonal anti-GFP (Chemicon, MAB3580, 1 : 1000). On the following day, slices were washed three times in PBS and treated with streptavidin and biotin according to the directions in the Vector streptavidin blocking kit. After blocking, slices were incubated for 2 h in a 1 : 300 dilution of goat anti-rabbit secondary antibody for GABA, TyH and ChAT, and in a 1 : 400 dilution of donkey anti-sheep secondary antibody for TrypH. Slices were washed two times in PBS and placed in a 1 : 3000 dilution of streptavidin–Cy3 (Jackson Laboratories) for 30 min. For mouse monoclonal anti-nNOS staining, a mouse-on-mouse kit (Vector BMK-2202) was used; 15−30 μg/mL streptavidin–Cy3 was applied for 5 min. For mouse monoclonal anti-GFP staining, an immunoperoxidase mouse-on-mouse kit was used (Vector PK2200); staining was revealed using diaminobenzidine (DAB). Slices were washed two times in PBS, mounted on subbed slides, air dried, and coverslipped using Vectarshield hardset mounting medium. Fluorescence microscopy was carried out with a Zeiss Axioplan 2 microscope and Slidebook software (Slide Book 4.1; Intelligent Imaging Innovations, Denver, CO, USA). Light microscopy of sections

stained with DAB was carried out using an Olympus BX51 microscope equipped with a SPOT RT color camera (Diagnostic Instruments Inc.).

Neurolucida analysis of the location of GFP-positive perikarya: light microscopy/GFP-positive cell mapping

The distribution of GFP-positive cells was examined in DAB-stained sections from four animals. In addition, the distribution of fluorescent GFP-positive cells was examined in slices from many other mice (including those used for double-staining against other neuronal markers). The distribution of cells did not vary among animals.

Following antibody tagging of GFP-positive neurons with the chromogen DAB, labeled cells were plotted, employing an Olympus BX51 microscope at ×20 magnification using the Neurolucida software (MicrobrightField, Williston, VT, USA). Representative schematics were generated from two sections from one animal, illustrating the distribution of GFP-positive neurons in REM sleep-related areas of the brainstem at the level of the DRN (Fig. 1A), and at the level of the LC (Fig. 1B). Neurolucida maps of labeled cells were then replotted on representative schematic coronal sections with Adobe Illustrator (Version 10), using sections adapted from the mouse brain atlas of Paxinos & Franklin (2001).

Fluorescent microscopy/GFP-positive and fluorescent cellular phenotype photography

Staining for each neuronal marker was conducted in three or four animals. A series of one in three coronal sections throughout the region of interest (−4.60 to −5.40 mm caudal to Bregma) was examined for colocalization of the marker with GFP. Slides of fluorescently labeled sections were viewed with the Zeiss Axioplan 2 microscope and Slidebook 3 software (Intelligent Imaging Innovations, Denver, CO, USA). GFP-positive cells were identified with excitation/emission at 488/509 nm (green fluorescence). Cy3-labeled neurons, conjugated to antibodies for ChAT, nNOS, TrypH, TyH, or GABA, were identified with excitation/emission at 590/617 nm (red fluorescence). Double-labeled neurons, as in the case of GFP-positive neurons (green fluorescence) and GABA–Cy3-positive cells (red fluorescence), were identified by the presence of both fluorescent signals in the cells, employing both filter sets. All the GFP- and GABA-positive neurons in the areas of interest from one representative animal were counted.

Digital images of fluorescently labeled neurons were captured with a Zeiss Axioplan 2/Slidebook 3 system at ×10 magnification, and montages of selected regions were constructed in Adobe Photoshop Elements, in order to illustrate entire brain regions where GFP and Cy3-labeled cells were located. The long-axis diameter of 50 randomly selected fluorescent neurons in selected regions (see Results) was measured using Slidebook software calibrated against a standard 25 μm grid. No corrections were made for potential shrinkage of the tissue, as we were only interested in comparing the size of neurons within the same areas of the same sections. However, cell diameters measured in this way were similar to those measured in living slices (in electrophysiology experiments).

Slice preparation for electrophysiological recordings

Slices for electrophysiological recordings were prepared at 10−12 a.m. from 8−13-day-old, heterozygous GAD67-GFP knock-in mice of either sex. The mice were deeply anesthetized with isofluorane and decapitated, and the brains were removed into ice-cold solution containing 209 mM sucrose, 1.8 mM KCl, 1.2 mM KH_2PO_4, 3.3 mM $MgSO_4$, 25.6 mM $NaHCO_3$ and 10 mM glucose. Three or four 200-μm-thick coronal brainstem slices were cut between −4.60 and −5.40 with respect to Bregma rostrocaudally [according to the atlas of Paxinos & Franklin (2001)], using a vibroslicer (Campden Instruments, UK). The slices were then placed into artificial cerebrospinal fluid containing 124 mM NaCl, 1.8 mM KCl, 1.2 mM KH_2PO_4,2 mM

$CaCl_2$, 1.3 mM $MgSO_4$, 25.6 mM $NaHCO_3$ and 10 mM glucose (osmolarity 300 mOsm), saturated with 95% O_2/5% CO_2 for ≥1 h at room temperature, and then transferred to the recording chamber (Warner Instruments, 27 L) at 32 °C, where they were constantly perfused with the same solution at a flow rate of 2−4 mL/min. The solution was warmed by passing it through an inline heater (Warner Instruments). The temperature of the solution was kept constant by a temperature controller (TC-344B; Warner Instruments) connected to the inline heater and receiving input from a thermistor placed in contact with the solution within the recording chamber.

Recording setup

The recording chamber was positioned under a Zeiss Axioskop 2 FS plus microscope fitted with ×4 air and ×63 water immersion objectives, a Hamamatsu ORCA-AR camera, and an EXFO Excite-120 fluorescence illumination system. The microscope was fitted with appropriate filters to provide the correct wavelengths of light for infrared illumination and GFP fluorescence (excitation/emission wavelength = 488/509 nm).

Whole-cell and cell-attached recordings

One slice was taken from the holding chamber, placed in the recording chamber, and held in place by two plastic meshes. The SubC (−5.20 to −5.40 mm caudal to Bregma) or PnO (−4.60 to −5.02 mm caudal to Bregma) were positioned in the center of the field of view by using the low-power (×4) objective. Subsequently, the slice was examined under the high-power (×63) water immersion objective, and a healthy neuron close to the surface of the slice was selected for recording on the basis of its appearance under infrared differential interference microscopy and expression of GFP fluorescence. Black-and-white images of the recorded neuron under infrared and fluorescence illumination were captured using the ORCA-AR camera and Wasabi imaging software (Hamamatsu). These images were calibrated using a 25 μm grid standard slide, and were used to measure the long and short diameter of the neurons.

Patch pipettes (3−6 MΩ, when filled with patch solution) were pulled from borosilicate glass (1B150F-4; World Precision Instruments, Sarasota, FL, USA) and filled with an intracellular 'patch' solution containing 130 mM potassium gluconate, 5 mM NaCl, 5 mM $MgCl_2$, 10 mM HEPES, 0.1 mM EGTA, 2 mM Na_2ATP, 0.5 mM NaGTP, 4 mM MgATP, 1 mM spermine, and 0.5% biocytin (pH 7.25 with KOH, 280 mOsm). Current was applied to the pipette, and the electrode potential and current were recorded using a Multiclamp 700 A amplifier (Axon Instruments, USA). Signals were digitized using a Digidata 1322 A analog-to-digital data acquisition device (Axon Instruments) and recorded on a PC using pClamp 9.0 software (Axon Instruments). Signals were digitized at 20 kHz and low-pass filtered at 10 kHz. Membrane potential measurements were adjusted for a −15 mV liquid junction potential between pipette and bath solutions (calculated using pClamp 9.0 software). Upon gaining access to the whole cell, series resistance was assessed in voltage-clamp mode from the peak value of current produced by an application of small (5 mV) voltage steps according to Ohm's law ($R = V/I$). Recordings were accepted if the series resistance was <20 MΩ and stable. Bridge balance [assessed by the application of small (10−50 pA) hyperpolarizing current pulses] was continuously maintained during current-clamp experiments. Continuous recordings of membrane voltage and current were made using a Gould TA11 chart recorder (Gould Electronics, Cleveland, USA) or a MiniDigi 1 A digital acquisition system and Axoscope 9.2 software (Axon Instruments) at 1 kHz.

Characterization of intrinsic membrane properties of GFP-positive neurons

The intrinsic membrane properties of the recorded neurons were characterized as follows. In current-clamp experiments, a series of 1 s current steps was applied to the neuron via the recording pipette. Each step was initiated from the resting membrane potential. The size of the

first (hyperpolarizing) step was adjusted so that the negative peak of the membrane potential during the step reached −115 to −120 mV. The delta step value was adjusted to be one-fifth of this value; that is, if $-x$ pA were required to attain −120 mV, then the size of each subsequent step (n) was $-x + n(|x|/5)$. After $n = 6$, the steps were depolarizing (positive current injection) and action potentials were elicited. The steps were continued until the firing rate did not increase further. The following parameters were determined: resting membrane potential, input resistance (determined from the negative peak of the smallest hyperpolarizing current step according to Ohm's law, $R = V/I$); membrane time constant [determined by fitting an exponential decay curve to the initial portion of the smallest hyperpolarizing current step; membrane potential = negative peak of membrane potential × exp(−t/tau)]; percentage depolarizing sag (determined from the largest hyperpolarizing step as membrane potential just before the end of the step/peak negativity during the step); and maximal firing rate (during last or penultimate depolarizing step – whichever is greater). The same series of steps was applied in the presence of the blocker of voltage-gated sodium channels, tetrodotoxin (TTX, 0.5 μM). The H-current blockers CsCl (2 mM) and ZD7288 (50 μM) and the calcium channel blocker $NiCl_2$ (500 μM) were bath applied.

Determination of the effects of bath-applied carbachol (CARB) and orexin A (Ox A)

In cell-attached recordings in voltage clamp, the membrane potential was clamped at −60 mV and the frequency of action potentials (observed as brief capacitative transients) was recorded online in 15 s bins using pClamp 9.0 software. Whole-cell current-clamp recordings were conducted as described above. Small 500 ms hyperpolarizing current pulses were applied every 15 s to monitor input resistance. At or shortly after the peak of the drug effect, current was applied to the cell to bring the membrane potential back to similar values as before the drug application, so as to be able to compare the resistance at the same membrane potential. CARB (10 μM) and Ox A (500 nM) were bath applied.

Post hoc *biocytin staining*

In whole-cell recordings, the neuron was filled with biocytin by diffusion from the patch pipette in order to confirm the location of the recorded neurons. In cell-attached recordings, at the end of the experiment we attempted to obtain a whole-cell recording from the same cell. When this was not possible, we withdrew the pipette from the slice and obtained a new whole-cell recording from the same cell from which the cell-attached recording had been made, using a fresh patch pipette. Following recording, the slice was fixed by placing it in a 4% buffered paraformaldehyde solution (Sigma) for 1−7 days. After treatment with 1% Triton X-100 for 2 h, the slices were treated with 3% H_2O_2 and 20% methanol for 4 min, washed twice in PBS, exposed to avidin–biotin complex (Vector) for 90 min, washed twice with PBS, and stained with DAB for 2−5 min. Following two additional washes with PBS, slices were dried, coverslipped, and photographed using a camera mounted to an upright microscope (Olympus BX51).

Drugs and statistics

Drugs were purchased from Sigma (St Louis, MO, USA). Stock solutions of drugs were prepared in distilled water at 1000 times their desired final concentrations and stored at −20 °C. Drugs were bath applied. The rate of flow of artificial cerebrospinal fluid was 3−4 mL/min, and there was a dead time of 1 min before substances entered the slice chamber. Data are presented as mean ± standard error of the mean. Statistical differences between control (immediately before drug application) and the peak of the drug effect (1.5−2.5 min after application) were tested using a paired Student's t-test. Data were analyzed and plotted using Graph Pad Prism 4.0 software.

Results

Distribution of GFP-positive neurons in REM sleep-related areas of the brainstem

GFP-positive somata were present throughout the brainstem. Green fluorescence was also present in the neuropil and within major fiber tracts, presumably due to the presence of GFP within dendrites and axons. GFP filled the somata (including the nucleus) and dendrites of the neurons, resulting in a continuous, homogeneous green fluorescence throughout the neuron. However, punctate green fluorescence, perhaps suggestive of axon terminals, was observed over the cell bodies of some GFP-positive and GFP-negative neurons. At the level of the DRN (Bregma AP −4.60 to −5.02; Fig. 1A), numerous small-sized (10−15 μm) GFP-positive neurons were present within the lateral wings of the DRN and laterodorsal tegmental nucleus (LDT), and also further laterally in the ventrolateral periaqueductal gray (vlPAG). Medium-sized (15 −25 μm) GFP-positive neurons were present among the fibers of the medial longitudinal fasciculus at the ventral border of the DRN/LDT/vlPAG and within the ventral tegmental nuclei of Gudden (VTg). Few GFP-positive neurons were present in the dorsal or dorsolateral periaqueductal gray, although numerous neurons were scattered uniformly throughout the surrounding inferior colliculi. Ventrolateral to the vlPAG, a moderate number of neurons were located in the lateral pontine tegmentum (LPT), including the cuneiform nucleus and the dorsal part of the pedunculopontine tegmental area (PPT), as well as among fiber tracts in the dorsolateral lemniscus. Ventral to the vlPAG, many small or mediumsized neurons were present in the dorsomedial tegmentum. In the median raphe nucleus (MRN), many small cells were located just lateral to the midline. Few neurons were located within the central part of the PnO. A moderate number of GFP-positive neurons were located in the ventromedial PnO, extending ventrolaterally out from the midline. A small number of scattered neurons were located in lateral and ventrolateral areas of the PnO just dorsal to the rostral periolivary region.

In sections labeled with TrypH to identify serotonergic neurons, several observations were made. First, GFP-positive neurons largely avoided the midline areas of the DRN and MRN, where serotonin neurons were most highly concentrated (Fig. 2). Second, most GFP-positive neurons were smaller than the TrypH-positive neurons in these areas (long-axis diameter 13.9 ± 0.2 μm for GFP-positive vs. 23.7 ± 0.7 μm for TrypH-positive in the DRN, $P \leq 0.001$; 12.1 ± 0.3 μm for GFP-positive vs. 17.8 ± 0.4 μm for TrypH-positive in the MRN, $P \leq 0.001$). Third, no TrypH-positive neurons were also GFP-positive in the DRN or MRN. In sections stained with ChAT to identify pontine cholinergic neurons (Fig. 3), small green fluorescent neurons were intermingled with larger ChAT-positive neurons in the laterodorsal and pedunculopontine tegmental nuclei (long-axis diameter 13.2 ± 0.2 μm for GFP-positive vs. 22.3 ± 0.5 μm for ChAT-positive in the LDT, $P \leq 0.001$; 13.4 ± 0.2 μm for GFP-positive vs. 21.5 ± 0.5 μm for ChAT-positive in the PPT, $P \leq 0.001$). GFP-positive neurons and fibers almost completely avoided the core of the mesencephalic motor trigeminal nucleus (Mo5; Fig. 3, A2). No ChAT and GFP double-labeled cells were observed.

At the level of the LC, LDT and SubC (Bregma −5.20 to −5.40; Figs 1B and 4), numerous small GFP-positive neurons were densely packed in the ovoid dorsal tegmental nuclei of Gudden, either side of the midline and in the surrounding central gray areas, including the LDT, but were not present in the core of the LC. A moderate number of small or medium-sized neurons were located in the alpha and dorsal parts of the SubC. More laterally, scattered GFP-positive neurons were located around the fibers of the superior cerebellar peduncle. As described previously (Li *et al.*, 2005), a ring of neurons was observed surrounding the Mo5. A moderate number of small to medium-sized neurons were present along the midline and in the ventral and ventrolateral portions of the reticular formation extending into the ventral SubC area. Fewer neurons were present within the core of the caudal reticular nucleus. Many neurons were labeled in the overlying cerebellar cortex (not shown).

In sections stained for TyH to identify catecholaminergic (noradrenergic) neurons, similar observations were made as in the DRN and MRN with TrypH staining (Fig. 4C). GFP-positive neurons surrounding the LC were smaller than the LC TyH-positive neurons (13.7 ± 0.3 μm for GFP-positive vs. 20.4 ± 0.6 μm for TyH-positive, $P \leq 0.001$), and the GFP-positive^{+} neurons were largely absent in the core of the LC. No TyH-positive/GFP-positive neurons were observed. In sections stained with nNOS or ChAT to identify pontine cholinergic neurons, small GFP-positive neurons were intermingled with large nNOS-positive or ChAT-positive neurons in the LDT (as described above). No nNOS-positive/GFP-positive or ChAT-positive/GFP-positive neurons were observed in the pons. However, in the medulla large, lightly stained nNOS-positive somata located along the midline of the reticular formation were found to be double-labeled for nNOS and GFP (ChAT-positive neurons were not present in this area).

GABA immunohistochemistry

To confirm that the GFP neurons were GABAergic in the regions that we used for electrophysiological recordings (SubC and PnO; see below), we performed fluorescent staining for GABA (Fig. 5). In the SubC, 81 of 84 (96%) GFP-positive neurons were found to be double-labeled for GABA, whereas in the ventral PnO, 69 of 70 (99%) of GFP-positive neurons were double-labeled. Similar results were found in other areas of the brainstem (data not shown). Thus, as in the cerebral cortex of these mice (Tamamaki *et al.*, 2003), essentially all the GFP-positive neurons in the upper brainstem can be considered to be GABAergic. Throughout the brainstem (−4.60 to −5.40 mm with respect to Bregma), 553 of 3459 (16%) of counted cells contained GABA but not GFP. These cells were of a similar size and morphology to neighboring GFP/GABA-positive cells, suggesting that GFP expression was too low to be detected in about 16% of GABA cells.

Intrinsic membrane properties of GFP-positive SubC and PnO neurons

Whole-cell or cell-attached recordings were made from 76 GFP-positive neurons in the SubC or PnO. The majority (55/76) of these neurons were small (10−15 μm) neurons. The remainder (21/76) were medium-sized (15−25 μm). Whole-cell recordings were made from 61 of these neurons. Small and medium-sized neurons in the SubC and PnO areas were similar in their intrinsic membrane properties, so the results have been pooled; the properties of these neurons are shown in Fig. 6. The neurons were spontaneously active in cell-attached or whole-cell current-clamp recordings, firing at 7.0 ± 0.4 Hz (Fig. 6A). Their input resistance was 692 ± 59 MΩ, and they had a membrane time constant of 38.1 ± 2.4 ms (n = 61). Action potentials had a threshold of −50.9 ± 0.8 mV, an amplitude of 62.7 ± 1.5 mV, and a rise time (threshold to peak) of 0.79 ± 0.04 ms. They were followed by monophasic afterhyperpolarizations with an amplitude of −19.8 ± 0.6 mV (with respect to the threshold potential). In the presence of TTX (0.5 μM), to block sodium-dependent action potentials, the resting membrane potential was −59.9 ± 1.0 mV (n = 59). During depolarizing current pulses, the neurons fired tonically, with little if any accommodation of firing (Fig. 6B). In those neurons tested with the full range of depolarizing current steps (see Materials and methods), the maximal firing rate was determined to be 50.8 ± 2.5 Hz (n = 53). During hyperpolarizing current injection, a medium-sized depolarizing sag (I_h) was observed (Fig. 6C; 74.8 ± 1.4% of the peak amplitude remaining at the end of a 1 s hyperpolarizing pulse to −120 mV, n 61; time constant 222 ± 20 ms) that was substantially or completely blocked by application of 2 mM CsCl (n = 8/8) or 50 μM ZD7288 (n = 7/7; Fig. 6C), indicating that it was mediated by opening of hyperpolarization-activated cation channels. In most neurons, this sag was only observed at potentials more negative than −80 mV, and is therefore unlikely to play a role in the spontaneous firing of these neurons. At the offset of hyperpolarizing current pulses, the neurons began firing either immediately (time from offset of largest hyperpolarizing current pulse to first spike = 38.1 ± 3.0 ms, n = 40) or with a short delay (142.4 ± 14.9 ms, n = 21). In the presence of TTX (0.5 μM), a small rebound depolarization (10.2 ± 1.0 mV, n = 21) was observed in those neurons that fired with a short

delay at the offset of hyperpolarizing current pulses (Fig. 6D), whereas in those with a longer delay, it was either much smaller or absent. This rebound depolarization was blocked by application of the calcium channel blocker $NiCl_2$ (500 μM, $n = 9/9$; Fig. 6D), suggesting that calcium channels, most likely of the low-threshold type, mediate this response. With larger hyperpolarizations, a residual rebound depolarization (1−3 mV) remained in the presence of $NiCl_2$, probably due to slow deactivation of the channels mediating the depolarizing sag (Pape, 1996).

GFP-positive neurons in the SubC and PnO exhibited TTX-insensitive inhibitory postsynaptic potentials that reversed around the chloride equilibrium potential (−70 mV under our conditions) and were blocked by the $GABA_A$ receptor antagonist bicuculline (10 μM, $n = 4$), indicating that these neurons are themselves under inhibitory control from other GABAergic neurons.

Responses of GFP-positive SubC neurons to the mixed cholinergic agonist CARB and Ox A

Application of $GABA_A$ receptor antagonists to the SubC or PnO region of rodents leads to the induction of a REM-like state (Boissard *et al.*, 2002; Pollock & Mistlberger, 2003; Sanford *et al.*, 2003). GABAergic neurons have been demonstrated in these areas in rats (Ford *et al.*, 1995; Boissard *et al.*, 2003), and as we show here, GABAergic (GFP-positive) neurons are also present in these areas in mice. As acetylcholine levels rise in the brainstem during REM sleep (Lydic *et al.*, 1991; Kodama *et al.*, 1992) and acetylcholine appears to act upstream of GABA in the control of REM sleep (Xi *et al.*, 2004), we hypothesized that these local neurons would be inhibited by the mixed cholinergic agonist CARB (i.e. REM-off) and excited by the REM-suppressing neurotransmitter Ox A (i.e. wake-on). We initially focused on the SubC area, as this area has been shown by a number of studies to be critical for REM muscle atonia (Mouret *et al.*, 1967; Morrison, 1988; Sanford *et al.*, 2001; Lu *et al.*, 2006) and is thus likely to be an important site where orexins act to prevent cataplexy.

We made cell-attached or whole-cell recordings from 30 GFP-positive SubC neurons. These neurons had a long-axis diameter of 13.4 ± 0.5 μm and a short-axis diameter of 8.8 ± 0.3 μm, and were usually ovoid or triangular in shape. An example of one of these neurons is shown in Fig. 7A; the location of the SubC area where recordings were made is illustrated in Fig. 7B. In cell-attached voltage-clamp recordings from GFP-positive SubC neurons held at −60 mV, capacitative transients reflecting spontaneous action potential firing were observed, allowing us to test the effects of CARB and Ox A without disturbing the intracellular milieu of the neurons. Application of CARB (10 μM) to these neurons increased the frequency of action potential firing from 7.0 ± 0.7 Hz to 10.6 ± 0.9 Hz ($n = 5$, $P < 0.05$; Fig. 7C). In a separate set of experiments in the whole-cell current-clamp recording mode in the presence of TTX (0.5 μM, CARB (10 μM) caused a depolarization of 5.6 ± 0.9 mV ($n = 5$; $P < 0.01$; Fig. 7D; −65.2 ± 3.0 mV to −59.6 ± 3.6 mV), which was associated with a nonsignificant decrease in input resistance to 90.0 ± 6.0% of control ($n = 4$, $P = 0.23$). Application of Ox A (500 nM) also increased the firing rate in cell-attached recordings from 6.4 ± 1.0 Hz to 11.0 ± 1.8 Hz ($n = 7$, $P < 0.05$; Fig. 7E). In whole-cell current-clamp recordings in the presence of TTX (0.5 μM), Ox A (500 nM) caused a depolarization of 7.0 ± 1.0 mV ($n = 5$; $P < 0.01$; Fig. 7F; −58.2 ± 3.4 mV to −51.2 ± 2.7 mV), which was associated with a nonsignificant increase in input resistance to 127.7 ± 9.4% of control ($n = 4$, $P = 0.13$).

Responses of GFP-positive PnO neurons to the mixed cholinergic agonist CARB and Ox A

As GFP-positive SubC neurons were not inhibited by CARB as we had hypothesized, we broadened our search to include the PnO region, which has also been shown to be an effective site where $GABA_A$ receptor antagonists can trigger a REM-like state in rodents (Sanford *et al.*, 2003). The PnO has also been shown to be sensitive to the REM-promoting effects of

cholinergic agonists or acetylcholinesterase inhibitors in rodents (Bourgin *et al.*, 1995; Marks & Birabil, 1998; Coleman *et al.*, 2004) and is important in controlling muscle tone even in infant rats (Gall *et al.*, 2007). The PnO has been shown to receive input from orexinergic neurons in the perifornical hypothalamus (Nunez *et al.*, 2006).

We made cell-attached and whole-cell recordings from 46 GFP-positive PnO neurons (mainly in the ventral and lateral parts of the PnO). These neurons had a long-axis diameter of 14.5 ± 0.5 μm and a short-axis diameter of 8.9 ± 0.3 μm, and like GFP-positive SubC neurons, were usually ovoid or triangular in shape. An example of one of these neurons is shown in Fig. 8A; the location of the PnO area where recordings were made is illustrated in Fig. 8B. As with GFP-positive SubC neurons, in cell-attached, voltage-clamp recordings from GFP-positive PnO neurons held at −60 mV, capacitative transients reflecting spontaneous action potential firing were observed. Twenty-three PnO neurons were tested with CARB (12 in cell-attached mode and 11 in whole-cell recordings). They were divided into two groups on the basis of their responses to CARB. In one group of GFP-positive PnO neurons tested in cell-attached mode (CARB-excited), application of CARB (10 μM) increased the frequency of action potential firing from 6.5 ± 0.9 Hz to 11.2 ± 1.2 Hz (n = 8/12, P < 0.01; Fig. 8C). In another group of GFP-positive PnO =neurons (CARB-inhibited), application of CARB (10 μM) decreased the frequency of action potential firing from 4.9 ± 1.0 Hz to 0.8 ± 0.7 Hz (n = 4/12, P < 0.05; Fig. 8E). Similarly, in a separate set of whole-cell current-clamp recordings in the presence of TTX (0.5 μM), CARB (10 μM) depolarized one group of neurons by 7.8 ± 1.5 mV (n = 7/11, P < 0.01; Fig. 8D; −61.7 ± 2.2 mV to −53.9 ± 1.4 mV). This depolarization was associated with variable changes in input resistance (97.3 ± 6.1% of control, n = 6, not significant). In other GFP-positive PnO neurons, CARB (10 μM) caused a hyperpolarization of 4.5 ± 0.6 mV (n = 4/11, P < 0.01; Fig. 8F; −54.8 ± 2.5 mV to −59.2 ± 2.6 mV). This hyperpolarization was associated with a decrease in input resistance to 74.0 ± 12.9% of control (n = 3, P = 0.2). No apparent differences in morphology, intrinsic membrane properties or location of neurons within the PnO were noted between those neurons that were excited and those that were inhibited by CARB.

Ox A (500 nM) excited all GFP-positive PnO neurons tested (including both CARB-excited and CARB-inhibited neurons). In cell-attached recordings, the firing rate was increased from 6.0 ± 0.7 Hz to 11.4 ± 1.8 Hz (n = 6, P < 0.05; Fig. 8G). In whole-cell current-clamp recordings in the presence of TTX (0.5 μM), Ox A (500 nM) caused a depolarization of 8.9 ± 1.6 mV (n = 9, P < 0.01; Fig. 8H; −58.4 ± 2.3 mV to −49.5 ± 1.5 mV) and increased input resistance to 133.0 ± 13.1% of control (n = 7, P < 0.05).

Discussion

The main findings of this study are as follows. First, GFP is expressed selectively in GABAergic neurons in the brainstem of GAD67-GFP knock-in mice. The presence of GFP within essentially all GABA neurons allowed us to provide the first comprehensive description of GABA neurons around the mesopontine junction in the mouse. Second, we report for the first time the intrinsic membrane properties of identified GABAergic neurons in the brainstem reticular formation and their responses to REM sleep neuromodulators. We found that the mixed cholinergic agonist CARB excites GABAergic neurons in the SubC, whereas it excites or inhibits different populations of GABAergic neurons in the PnO. In contrast, we report that Ox A excites all GABAergic neurons in the SubC and PnO.

In the heterozygous knock-in mice used here, GFP has been knocked in to the native GAD67 gene so that it is under the control of the full GAD67 promoter region, and thus should be expressed in all GABA neurons (Tamamaki *et al.*, 2003). In contrast, another mouse model expressing GFP in inhibitory neurons (GIN mice) used only part of the GAD67 promoter region

to direct expression, and only a subpopulation of GABA neurons were labeled with GFP (Oliva *et al.*, 2000). Furthermore, the construct used to drive expression in GIN mice was inserted randomly multiple times into the mouse genome, leaving open the possibility of position effects leading to ectopic expression. In the GAD67-GFP knock-in mice used here, GABA or GAD67 immunohistochemistry revealed that GFP is expressed exclusively in GABAergic cell bodies and processes in the cerebral cortex, hippocampus, arcuate nucleus, superior colliculus and inferior colliculus (Tamamaki *et al.*, 2003; Acuna-Goycolea *et al.*, 2005; Ono *et al.*, 2005; Tsunekawa *et al.*, 2005; Hoskison *et al.*, 2007). Our results and those of Li *et al.* (2005) suggest that this is also the case in the upper brainstem. To the best of our knowledge, a comprehensive distribution of GABA neurons around the mesopontine junction of the mouse has not been published. However, the distribution of GFP-positive neurons in knock-in mice paralleled the distribution of GAD-positive neurons previously described in the rat (Ford *et al.*, 1995), and was similar to the distribution of GAD67 neurons in the mouse brainstem as revealed by *in situ* hybridization (unpublished observations). GFP-positive neurons were mostly small neurons (10−15 μm in diameter) whose size contrasted with that of the larger neighboring reticular, aminergic or cholinergic neurons. Similar findings were found with respect to GABA-positive somata in the ventral part of the PnO in the cat (De La Roza & Reinoso-Suarez, 2006). In contrast to results reported previously in the cat (Jia *et al.*, 2003), no nNOS-positive (presumably cholinergic) neurons in the mouse LDT or PPT were GFP-positive, although a small number of larger-sized (noncholinergic) neurons in the medulla were found to contain GFP and nNOS. Similarly, no catecholaminergic neurons in the LC/SubC or serotonergic neurons in the DRN or MRN were double-labeled for TyH/GFP or TrypH/GFP, respectively. As shown previously in the rat (Maloney *et al.*, 1999, 2000; Gervasoni *et al.*, 2000; Boissard *et al.*, 2003; De La Roza & Reinoso-Suarez, 2006; Lu *et al.*, 2006), GABAergic (GFP-positive) neurons were present in areas controlling REM sleep, including the DRN/vlPAG, LPT, central gray surrounding the LDT and LC, as well as in the PnO and SubC regions of the reticular formation. Staining for GABA confirmed that essentially all GFP-positive neurons in the brainstem are GABAergic, whereas around 16% of GABA neurons have undetectable levels of GFP. A similar percentage of neurons with GFP expression to low too detect was found in other mouse models utilizing GFP, e.g. orexin GFP mice (19%) (Li *et al.*, 2002).

As a first step towards understanding the properties of brainstem GABA neurons involved in REM sleep control, we focused on the SubC and PnO regions, as injections of $GABA_A$ receptor agonists or antagonists into these regions of rodents have been shown to profoundly modify the amount of REM sleep (Boissard *et al.*, 2002; Sanford *et al.*, 2003). We performed whole-cell recordings from GFP-positive neurons in thin slices prepared from neonatal (8−13-day-old) animals. In mice or rats of this age, the adult sleep–wake cycle is not fully established. However, it has recently been shown in the rat by Blumberg and colleagues that most of the brainstem features of adult REM sleep are present in rodents by postnatal days 8−13 (Karlsson *et al.*, 2005). In particular, muscle atonia during active sleep (interrupted by muscle twitches initiated spinally or supraspinally) is present by postnatal day 8, the age of the youngest animal used (Karlsson & Blumberg, 2002). Furthermore, the same pontine and medullary sites involved in muscle atonia appear to be active in postnatal day 8 animals as in the adult (Karlsson *et al.*, 2005). Fewer studies have investigated the ontogeny of sleep in the mouse; however, the development of the sleep–wake cycle in mice appears to parallel quite closely the development of the sleep–wake cycle in the rat (Daszuta *et al.*, 1983; Daszuta & Gambarelli, 1985). Thus, we believe that our results are relevant for an understanding of REM sleep control.

GFP-positive neurons in the PnO/SubC regions had similar intrinsic electrophysiological properties as other reticular formation neurons in these areas (Gerber *et al.*, 1989; Nunez *et al.*, 1997; Brown *et al.*, 2006c), emphasizing the utility of having a way to identify GABAergic neurons prior to recording. GFP-positive neurons fired spontaneously without adaptation and were fast-spiking. Thus, unless inhibited by fast synaptic inputs or neuromodulators, they will

exert a constant inhibitory tone upon the neurons that they innervate. They had a depolarizing sag during hyperpolarizing current pulses that was blocked by 2 mM extracellular caesium or 50 μM ZD7288 and is thus probably mediated by hyperpolarization-activated cation channels. Most neurons also had a rebound depolarization at the offset of hyperpolarizing current pulses, due to activation of low-threshold calcium channels (nickel-sensitive) and delayed deactivation of the channels mediating the depolarizing sag. This rebound was not large enough to cause burst firing, but allowed the neurons to begin firing with only a short delay following hyperpolarization. Overall, the intrinsic membrane properties of neurons in the SubC/PnO were similar to those of tonic firing GFP-positive neurons recorded in the inferior colliculus of GAD67-GFP knock-in mice (Ono *et al.*, 2005). The mechanisms underlying spontaneous firing in these neurons await further investigation, but are unlikely to include a role for I_h,as a depolarizing sag was only observed at potentials considerably more negative than the resting membrane potential.

In cats, cholinergic agonists consistently promote REM sleep, and acetylcholine levels rise during this state [reviewed in McCarley (2004, 2007)]. In rodents, however, the role of cholinergic neurons in promoting REM sleep has recently been challenged (Boissard *et al.*, 2002; Verret *et al.*, 2005). As discussed previously (Brown *et al.*, 2006c), at least part of the difference between cats and rodents with respect to cholinergic agonist effects may reflect difficulties in precisely localizing injections of pharmacological agents in the smaller rodent brain. However, if real species differences exist, then they should be apparent in the postsynaptic actions of acetylcholine on REM-promoting or REM-inhibiting neurons. As a first step towards understanding the effects of acetycholine on GABA neurons in REM-related brainstem areas, we tested the effects of the mixed cholinergic agonist, CARB, on the firing and membrane potential of GFP-positive neurons. The effects of CARB and Ox A persisted in the presence of TTX, indicating that they acted directly on the postsynaptic membrane. Changes in input resistance with CARB and with Ox A were variable, although inhibitory effects of CARB and excitatory effects of Ox A were normally associated with decreases and increases in input resistance, respectively, suggesting an involvement of potassium channels. The mechanisms underlying these effects, particularly the excitations, are likely to be complex and may involve actions on cation channels as well as potassium channels, as observed for orexin-mediated excitations in the DRN (Brown *et al.*, 2002).

In the SubC, contrary to our expectations, CARB excited GFP-positive neurons, suggesting that they are REM-on neurons. Recent findings in the rat using Fos immunohistochemistry, showing an increased number of Fos-positive/GAD67-positive neurons within the SubC region during REM-rich periods, support this idea (Maloney *et al.*, 1999; Lu *et al.*, 2006). GABAergic neurons surrounding the LC have been found to synapse on LC noradrenaline neurons (Aston-Jones *et al.*, 2004), and increased GABA levels have been reported in this region during REM (Nitz & Siegel, 1997b). Taken together, these data suggest that CARB-excited GFP-positive SubC neurons project to and inhibit LC noradrenaline neurons during REM (McCarley, 2007). SubC GABA neurons have also recently been shown to be reciprocally connected to REM-off GABAergic neurons in the LPT (Lu *et al.*, 2006). As we show here, they exhibit spontaneous inhibitory synaptic potentials, confirming electrophysiologically that they receive inputs from other GABAergic neurons and consistent with the presence of punctate staining on their somata, suggestive of axon terminals. Surprisingly, in view of our expectations, CARB-excited GFP-positive neurons were also found within the PnO (15/23 = 65% of cells tested), a site where CARB has been shown to be effective in enhancing the amount of REM sleep in rodents (Bourgin *et al.*, 1995; Marks & Birabil, 1998). Gervasoni *et al.* (2000) have shown that the PnO provides GABAergic afferents to the DRN. It is thus possible that these neurons are involved in turning off DRN serotonin neurons during REM.

With respect to the possible roles of the CARB-inhibited neurons in the PnO (8/23 = 35% of cells tested), we have suggested that these neurons are involved in suppressing the firing of REM-on reticular neurons in the PnO and/or SubC (McCarley, 2007). Our preliminary data using anatomical tracing techniques in the GAD67-GFP knock-in mice support the idea that PnO GABA neurons project to the SubC (Brown *et al.*, 2006a), and hence their inhibition by cholinergic projections during REM would disinhibit muscle atonia-on neurons in the SubC. These CARB-inhibited neurons may thus be one part of a distributed network of GABAergic neurons within the brainstem, acting to suppress muscle atonia and other aspects of REM sleep during waking (Maloney *et al.*, 2000; Boissard *et al.*, 2003; Xi *et al.*, 2004; Lu *et al.*, 2006). These hypotheses need to be tested in future anatomical studies and experiments using selective lesioning of GABAergic neurons in these different parts of the brainstem.

Elsewhere in the brain, GABAergic neurons are prominent targets for the orexins, which excite presumed or identified GABAergic neurons in the DRN (Liu *et al.*, 2002), substantia nigra pars reticulata (Korotkova *et al.*, 2002), ventral tegmental area of Tsai (Korotkova *et al.*, 2003), arcuate nucleus (Burdakov *et al.*, 2003), and medial septum (Wu *et al.*, 2002). We show here that Ox A also excites reticular formation GABA neurons in the SubC and PnO. The orexin excitation of CARB-inhibited neurons was expected, as these neurons are presumably involved in suppressing the firing of glutamatergic REM-on neurons. However, the excitation by Ox A of CARB-excited neurons appears to be less directly interpretable. Apparently, orexins directly excite and at the same time increase the GABAergic input to REM-off aminergic neurons in the DRN and LC (Brown *et al.*, 2002; Liu *et al.*, 2002). Presumably, the direct postsynaptic effects of orexins on aminergic neurons (Brown *et al.*, 2001, 2002; Liu *et al.*, 2002) outweigh the indirect inhibitory actions during waking. During REM, when orexin levels and postsynaptic effects should be reduced or absent, CARB excitation of inhibitory inputs will lead to the reduced activity of aminergic neurons typical of this state. Further complicating our understanding of brainstem orexin effects is one study showing that orexins excited presumed glutamatergic, REM-on reticular formation neurons (Xi *et al.*, 2002). Thus, the brainstem actions of orexins are complex and warrant further investigation.

Although we propose here that SubC and PnO GFP-positive neurons are projection neurons, we note that other possibilities exist. For instance, they could also be local interneurons inhibiting neighboring reticular neurons. In fact, one recent in vivo study in rats has shown that Ox A (hypocretin-1) inhibits PnO neurons and that this inhibition is blocked by the $GABA_A$ antagonist bicuculline (Nunez *et al.*, 2006), indicating that it was mediated through activation of $GABA_A$ receptors (secondary to increased activity in GABAergic somata or afferent axons). This result would also be consistent with our finding of Ox A excitation of PnO GABA neurons.

In conclusion, we show here that the GAD67-GFP knock-in mouse is a useful model for investigating the role of GABAergic neurons in the control of REM sleep (and other states). We propose that acetylcholine inhibition of a subset of GABAergic neurons is likely to promote the induction of REM sleep via disinhibition of REM active neurons and inhibition of REM-off neurons, whereas orexinergic suppression of REM during waking is likely to be mediated in part by excitation of acetylcholine-inhibited GABAergic neurons.

Acknowledgements

This work was supported by the Veterans Administration Medical Research and by NIMH R01 MH062522 and NIMH R37 MH039683 (to R. W. McCarley) and Grants-in-Aids for Scientific Research from MEXT and MHLW, Japan (to Y. Yanagawa). We would like to thank Brianne Jeffrey for excellent technical assistance.

References

Acuna-Goycolea C, Tamamaki N, Yanagawa Y, Obata K, van den Pol AN. Mechanisms of neuropeptide Y, peptide YY, and pancreatic polypeptide inhibition of identified green fluorescent protein-expressing

GABA neurons in the hypothalamic neuroendocrine arcuate nucleus. J. Neurosci 2005;25:7406–7419. [PubMed: 16093392]

Asada H, Kawamura Y, Maruyama K, Kume H, Ding R, Ji FY, Kanbara N, Kuzume H, Sanbo M, Yagi T, Obata K. Mice lacking the 65 kDa isoform of glutamic acid decarboxylase (GAD65) maintain normal levels of GAD67 and GABA in their brains but are susceptible to seizures. Biochem. Biophys. Res. Commun 1996;229:891–895. [PubMed: 8954991]

Asada H, Kawamura Y, Maruyama K, Kume H, Ding RG, Kanbara N, Kuzume H, Sanbo M, Yagi T, Obata K. Cleft palate and decreased brain gamma-aminobutyric acid in mice lacking the 67-kDa isoform of glutamic acid decarboxylase. Proc. Natl Acad. Sci. USA 1997;94:6496–6499. [PubMed: 9177246]

Aston-Jones G, Zhu Y, Card JP. Numerous GABAergic afferents to locus ceruleus in the pericerulear dendritic zone: possible interneuronal pool. J. Neurosci 2004;24:2313–2321. [PubMed: 14999082]

Boissard R, Gervasoni D, Schmidt MH, Barbagli B, Fort P, Luppi PH. The rat ponto-medullary network responsible for paradoxical sleep onset and maintenance: a combined microinjection and functional neuroanatomical study. Eur. J. Neurosci 2002;16:1959–1973. [PubMed: 12453060]

Boissard R, Fort P, Gervasoni D, Barbagli B, Luppi PH. Localization of the GABAergic and non-GABAergic neurons projecting to the sublaterodorsal nucleus and potentially gating paradoxical sleep onset. Eur. J. Neurosci 2003;18:1627–1639. [PubMed: 14511341]

Bourgin P, Escourrou P, Gaultier C, Adrien J. Induction of rapid eye movement sleep by carbachol infusion into the pontine reticular formation in the rat. Neuroreport 1995;6:532–536. [PubMed: 7766858]

Brown RE, Sergeeva OA, Eriksson KS, Haas HL. Orexin A excites serotonergic neurons in the dorsal raphe nucleus of the rat. Neuropharmacology 2001;40:457–459. [PubMed: 11166339]

Brown RE, Sergeeva OA, Eriksson KS, Haas HL. Convergent excitation of dorsal raphe serotonin neurons by multiple arousal systems (orexin/hypocretin, histamine and noradrenaline). J. Neurosci 2002;22:8850–8859. [PubMed: 12388591]

Brown RE, Thakkar MM, Winston S, Basheer R, Yanagawa Y, McCarley RW. Characterization of brainstem GABAergic neurons controlling rapid-eye-movement (REM) sleep in GAD67-GFP knock-in mice. FENS Abstract 2006a;3:A114.3.

Brown RE, Winston S, Basheer R, Yanagawa Y, Thakkar M, McCarley RW. Electrophysiological recordings from brainstem GABAergic neurons in GAD67-GFP knock-in mice and REM sleep control by cholinergic and orexinergic mechanisms. Sleep 2006b;29:A45.

Brown RE, Winston S, Basheer R, Thakkar MM, McCarley RW. Electrophysiological characterization of neurons in the dorsolateral pontine rapid-eye-movement sleep induction zone of the rat: intrinsic membrane properties and responses to carbachol and orexins. Neuroscience 2006c;143:739–755. [PubMed: 17008019]

Burdakov D, Liss B, Ashcroft FM. Orexin excites GABAergic neurons of the arcuate nucleus by activating the sodium–calcium exchanger. J. Neurosci 2003;23:4951–4957. [PubMed: 12832517]

Coleman CG, Lydic R, Baghdoyan HA. M2 muscarinic receptors in pontine reticular formation of C57BL/6J mouse contribute to rapid eye movement sleep generation. Neuroscience 2004;126:821–830. [PubMed: 15207317]

Daszuta A, Gambarelli F, Ternaux JP. Sleep variations in C57BL and BALBc mice from 3 weeks to 14 weeks of age. Brain Res 1983;283:87–96. [PubMed: 6831259]

Daszuta A, Gambarelli F. Early postnatal development of EEG and sleep–waking cycle in two inbred mouse strains. Brain Res 1985;354:39–47. [PubMed: 4041918]

De La Roza C, Reinoso-Suarez F. GABAergic structures in the ventral part of the ora pontine reticular nucleus: an ultrastructural immunogold analysis. Neuroscience 2006;142:1183–1193. [PubMed: 16916586]

Esclapez M, Tillakaratne NJ, Tobin AJ, Houser CR. Comparative localization of mRNAs encoding two forms of glutamic acid decarboxylase with nonradioactive in situ hybridization methods. J. Comp. Neurol 1993;331:339–362. [PubMed: 8514913]

Esclapez M, Tillakaratne NJ, Kaufman DL, Tobin AJ, Houser CR. Comparative localization of two forms of glutamic acid decarboxylase and their mRNAs in rat brain supports the concept of functional differences between the forms. J. Neurosci 1994;14:1834–1855. [PubMed: 8126575]

Ford B, Holmes CJ, Mainville L, Jones BE. GABAergic neurons in the rat pontomesencephalic tegmentum: codistribution with cholinergic and other tegmental neurons projecting to the posterior lateral hypothalamus. J. Comp. Neurol 1995;363:177–196. [PubMed: 8642069]

Gall AJ, Poremba A, Blumberg MS. Brainstem cholinergic modulation of muscle tone in infant rats. Eur. J. Neurosci 2007;25:3367–3375. [PubMed: 17553005]

Gerber U, Greene RW, McCarley RW. Repetitive firing properties of medial pontine reticular formation neurones of the rat recorded in vitro. J. Physiol 1989;410:533–560. [PubMed: 2795489]

Gervasoni D, Darracq L, Fort P, Souliere F, Chouvet G, Luppi PH. Electrophysiological evidence that noradrenergic neurons of the rat locus coeruleus are tonically inhibited by GABA during sleep. Eur. J. Neurosci 1998;10:964–970. [PubMed: 9753163]

Gervasoni D, Peyron C, Rampon C, Barbagli B, Chouvet G, Urbain N, Fort P, Luppi PH. Role and origin of the GABAergic innervation of dorsal raphe serotonergic neurons. J. Neurosci 2000;20:4217–4225. [PubMed: 10818157]

Hoskison MM, Yanagawa Y, Obata K, Shuttleworth CW. Calcium-dependent NMDA-induced dendritic injury and MAP2 loss in acute hippocampal slices. Neuroscience 2007;145:66–79. [PubMed: 17239543]

Jia HG, Yamuy J, Sampogna S, Morales FR, Chase MH. Colocalization of gamma-aminobutyric acid and acetylcholine in neurons in the laterodorsal and pedunculopontine tegmental nuclei in the cat: a light and electron microscopic study. Brain Res 2003;992:205–219. [PubMed: 14625059]

Karlsson KA, Blumberg MS. The union of the state: myoclonic twitching is coupled with nuchal muscle atonia in infant rats. Behav. Neurosci 2002;116:912–917. [PubMed: 12369810]

Karlsson KA, Gall AJ, Mohns EJ, Seelke AM, Blumberg MS. The neural substrates of infant sleep in rats. PLoS Biol 2005;3:e143. [PubMed: 15826218]

Kodama T, Lai YY, Siegel JM. Enhancement of acetylcholine release during REM sleep in the caudomedial medulla as measured by in vivo microdialysis. Brain Res 1992;580:348–350. [PubMed: 1504813]

Korotkova TM, Eriksson KS, Haas HL, Brown RE. Selective excitation of GABAergic neurons in the substantia nigra of the rat by orexin/hypocretin in vitro. Regul. Pept 2002;104:83–89. [PubMed: 11830281]

Korotkova TM, Sergeeva OA, Eriksson KS, Haas HL, Brown RE. Excitation of ventral tegmental area dopaminergic and nondopaminergic neurons by orexins/hypocretins. J. Neurosci 2003;23:7–11. [PubMed: 12514194]

Li Y, Gao XB, Sakurai T, van den Pol AN. Hypocretin/orexin excites hypocretin neurons via a local glutamate neuron-A potential mechanism for orchestrating the hypothalamic arousal system. Neuron 2002;36:1169–1181. [PubMed: 12495630]

Li JL, Wu SX, Tomioka R, Okamoto K, Nakamura K, Kaneko T, Mizuno N. Efferent and afferent connections of GABAergic neurons in the supratrigeminal and the intertrigeminal regions. An immunohistochemical tract-tracing study in the GAD67-GFP knock-in mouse. Neurosci. Res 2005;51:81–91. [PubMed: 15596244]

Liu RJ, Van den Pol AN, Aghajanian GK. Hypocretins (orexins) regulate serotonin neurons in the dorsal raphe nucleus by excitatory direct and inhibitory indirect actions. J. Neurosci 2002;22:9453–9464. [PubMed: 12417670]

Lu J, Sherman D, Devor M, Saper CB. A putative flip-flop switch for control of REM sleep. Nature 2006;441:589–594. [PubMed: 16688184]

Luppi PH, Gervasoni D, Boissard R, Verret L, Goutagny R, Peyron C, Salvert D, Leger L, Barbagli B, Fort P. Brainstem structures responsible for paradoxical sleep onset and maintenance. Arch. Ital. Biol 2004;142:397–411. [PubMed: 15493544]

Lydic R, Baghdoyan HA, Lorinc Z. Microdialysis of cat pons reveals enhanced acetylcholine release during state-dependent respiratory depression. Am. J. Physiol 1991;261:R766–R770. [PubMed: 1887963]

Maloney KJ, Mainville L, Jones BE. Differential c-Fos expression in cholinergic, monoaminergic, and GABAergic cell groups of the pontomesencephalic tegmentum after paradoxical sleep deprivation and recovery. J. Neurosci 1999;19:3057–3072. [PubMed: 10191323]

Maloney KJ, Mainville L, Jones BE. c-Fos expression in GABAergic, serotonergic, and other neurons of the pontomedullary reticular formation and raphe after paradoxical sleep deprivation and recovery. J. Neurosci 2000;20:4669–4679. [PubMed: 10844036]

Marks GA, Birabil CG. Enhancement of rapid eye movement sleep in the rat by cholinergic and adenosinergic agonists infused into the pontine reticular formation. Neuroscience 1998;86:29–37. [PubMed: 9692741]

McCarley RW. Mechanisms and models of REM sleep control. Arch. Ital. Biol 2004;142:429–467. [PubMed: 15493547]

McCarley RW. Neurobiology of REM and NREM sleep. Sleep Med 2007;8:302–330. [PubMed: 17468046]

Morrison AR. Paradoxical sleep without atonia. Arch. Ital. Biol 1988;126:275–289. [PubMed: 3058081]

Mouret J, Delorme F, Jouvet M. Lesions of the pontine tegmentum and sleep in rats. C. R. Seances Soc. Biol. Fil 1967;161:1603–1606. [PubMed: 4231637]

Nitz D, Siegel J. GABA release in the dorsal raphe nucleus: role in the control of REM sleep. Am. J. Physiol 1997a;273:R451–R455. [PubMed: 9249585]

Nitz D, Siegel JM. GABA release in the locus coeruleus as a function of sleep/wake state. Neuroscience 1997b;78:795–801. [PubMed: 9153658]

Nunez A, De la Roza C, Rodrigo-Angulo ML, Buno W, Reinoso-Suarez F. Electrophysiological properties and cholinergic responses of rat ventral oral pontine reticular neurons in vitro. Brain Res 1997;754:1–11. [PubMed: 9134953]

Nunez A, Moreno-Balandran ME, Rodrigo-Angulo ML, Garzon M, De Andres I. Relationship between the perifornical hypothalamic area and oral pontine reticular nucleus in the rat. Possible implication of the hypocretinergic projection in the control of rapid eye movement sleep. Eur. J. Neurosci 2006;24:2834–2842. [PubMed: 17116163]

Oliva AA, Jiang M, Lam T, Smith KL, Swann JW. Novel hippocampal interneuronal subtypes identified using transgenic mice that express green fluorescent protein in GABAergic interneurons. J. Neurosci 2000;20:3354–3368. [PubMed: 10777798]

Ono M, Yanagawa Y, Koyano K. GABAergic neurons in inferior colliculus of the GAD67-GFP knock-in mouse: electrophysiological and morphological properties. Neurosci. Res 2005;51:475–492. [PubMed: 15740810]

Pape HC. Queer current and pacemaker: the hyperpolarization-activated cation current in neurons. Annu. Rev. Physiol 1996;58:299–327. [PubMed: 8815797]

Paxinos, G.; Franklin, KBJ. The Mouse Brain in Stereotaxic Coordinates. Academic Press; San Diego, CA: 2001.

Pollock MS, Mistlberger RE. Rapid eye movement sleep induction by microinjection of the GABA-A antagonist bicuculline into the dorsal subcoeruleus area of the rat. Brain Res 2003;962:68–77. [PubMed: 12543457]

Sanford LD, Cheng CS, Silvestri AJ, Tang X, Mann GL, Ross RJ, Morrison AR. Sleep and behaviour in rats with pontine lesions producing REM without atonia. Sleep Res. Online 2001;4:1–5.

Sanford LD, Tang X, Xiao J, Ross RJ, Morrison AR. GABAergic regulation of REM sleep in reticularis pontis oralis and caudalis in rats. J. Neurophysiol 2003;90:938–945. [PubMed: 12672782]

Tamamaki N, Yanagawa Y, Tomioka R, Miyazaki J, Obata K, Kaneko T. Green fluorescent protein expression and colocalization with calretinin, parvalbumin, and somatostatin in the GAD67-GFP knock-in mouse. J. Comp. Neurol 2003;467:60–79. [PubMed: 14574680]

Thakkar MM, Tao R, Yunren B, Winston S, Chen L, McCarley RW. GABA release in the pontine reticular formation is lowest during REM sleep. Soc. Neurosci. Abstract 2004:895.5.

Torterolo P, Yamuy J, Sampogna S, Morales FR, Chase MH. GABAergic neurons of the cat dorsal raphe nucleus express c-fos during carbachol-induced active sleep. Brain Res 2000;884:68–76. [PubMed: 11082488]

Torterolo P, Yamuy J, Sampogna S, Morales FR, Chase MH. GABAergic neurons of the laterodorsal and pedunculopontine tegmental nuclei of the cat express c-fos during carbachol-induced active sleep. Brain Res 2001;892:309–319. [PubMed: 11172778]

Tsunekawa N, Yanagawa Y, Obata K. Development of GABAergic neurons from the ventricular zone in the superior colliculus of the mouse. Neurosci. Res 2005;51:243–251. [PubMed: 15710488]

Verret L, Leger L, Fort P, Luppi P-H. Cholinergic and noncholinergic brainstem neurons expressing Fos after paradoxical (REM) sleep deprivation and recovery. Eur. J. Neurosci 2005;21:2488–2504. [PubMed: 15932606]

Wu M, Zhang Z, Leranth C, Xu C, Van den Pol AN, Alreja M. Hypocretin increases impulse flow in the septohippocampal GABAergic pathway: implications for arousal via a mechanism of hippocampal disinhibition. J. Neurosci 2002;22:7754–7765.

Xi MC, Morales FR, Chase MH. Evidence that wakefulness and REM sleep are controlled by a GABAergic pontine mechanism. J. Neurophysiol 1999;82:2015–2019. [PubMed: 10515993]

Xi MC, Fung SJ, Yamuy J, Morales FR, Chase MH. Induction of active (REM) sleep and motor inhibition by hypocretin in the nucleus pontis oralis of the cat. J. Neurophysiol 2002;87:2880–2888. [PubMed: 12037191]

Xi MC, Morales FR, Chase MH. Interactions between GABAergic and cholinergic processes in the nucleus pontis oralis: neuronal mechanisms controlling active (rapid eye movement) sleep and wakefulness. J. Neurosci 2004;24:10670–10678. [PubMed: 15564583]

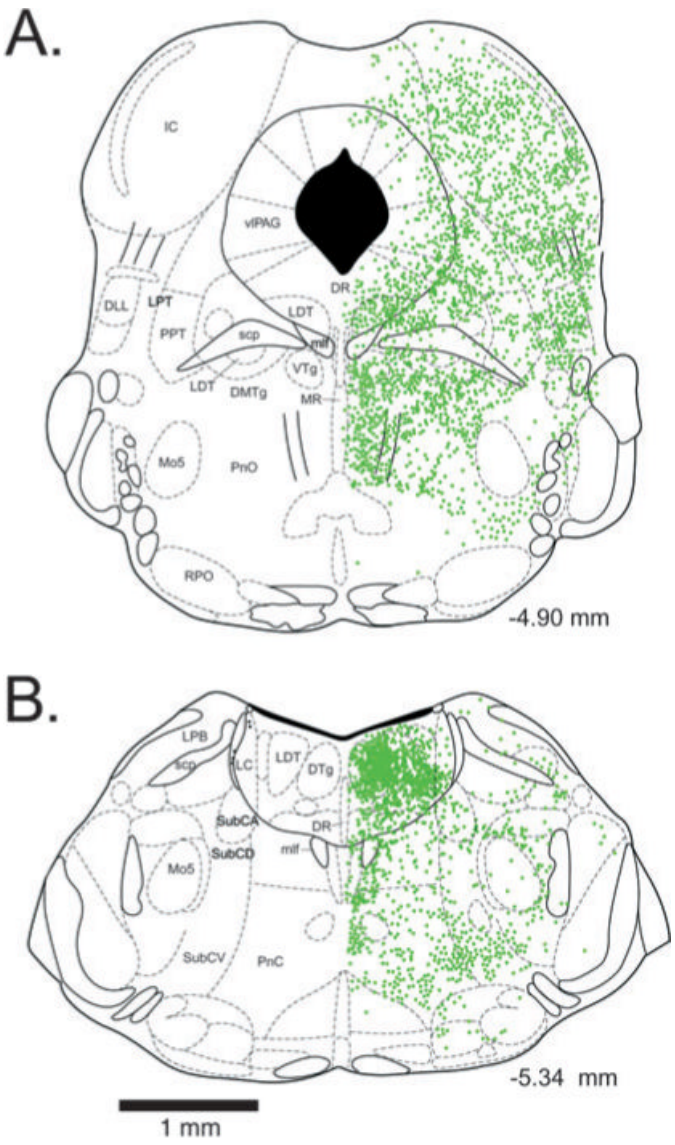

Fig. 1.

Location of green fluorescent protein-positive neuronal perikarya in the brainstem of GAD67-GFP knock-in mice at the level of the dorsal raphe nucleus (A) and locus coeruleus (B). Numbers indicate the rostrocaudal location of the section with respect to Bregma. DLL, dorsolateral lemniscus; DMTg, dorsomedial tegmental area; DTg, dorsal tegmental nucleus of Gudden; DR, dorsal raphe nucleus; IC, inferior colliculus; LC, locus coeruelus; LDT, laterodorsal tegmentum; LPB, lateral parabrachial nucleus; LPT, lateral pontine tegmentum; mlf, medial longitudinal fasciculus; Mo5, motor trigeminal nucleus; MR, median raphe nucleus; PnC, pontine reticular nucleus, caudal part; PnO, pontine nucleus oralis; PPT, pedunculopontine tegmental area; RPO, rostral periolivary region; scp, superior cerebellar peduncle; SubCA, subcoeruleus nucleus, alpha part; SubCD, subcoeruleus nucleus, dorsal part; SubCV, subcoeruleus nucleus, ventral part; vlPAG, ventrolateral periaqueductal gray; VTg, ventral tegmental nucleus of Gudden.

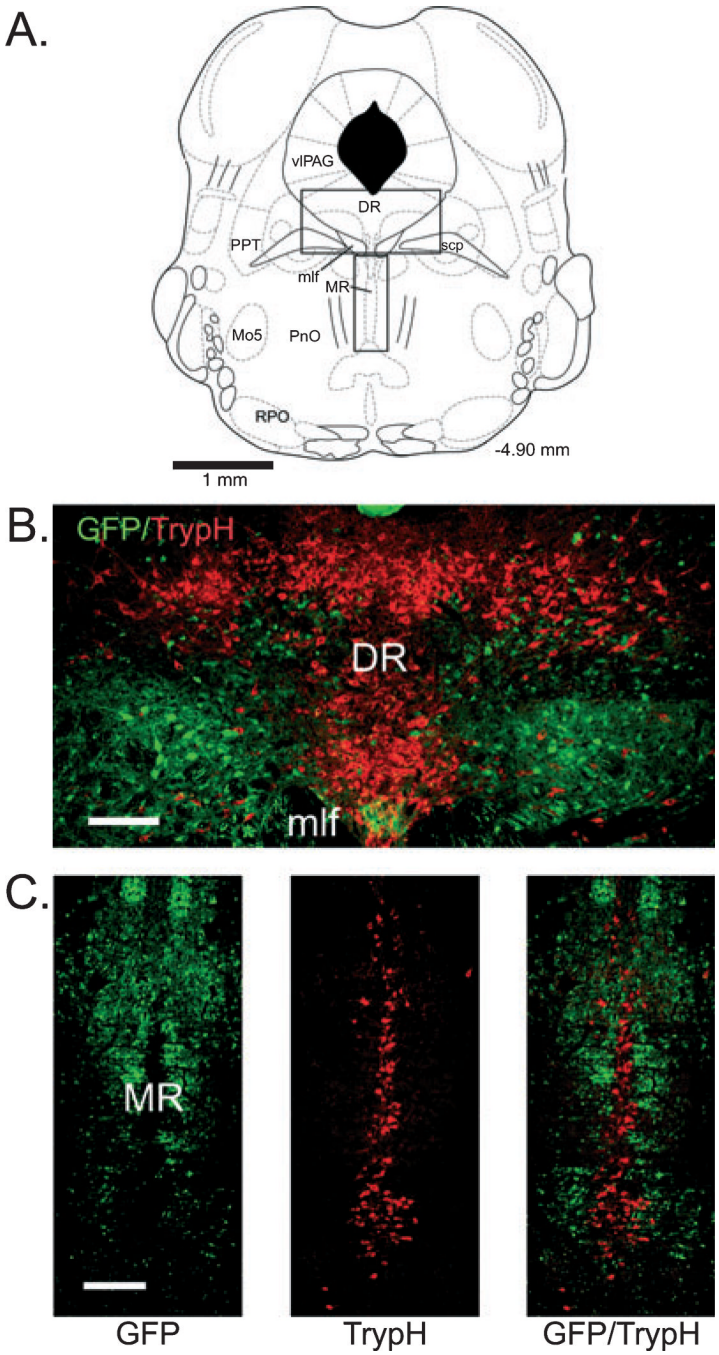

Fig. 2.

Green fluorescent protein (GFP)-positive neurons have a complementary distribution to serotonergic neurons in the dorsal and median raphe. (A) Schematic indicating the locations (rectangles) of the dorsal raphe (DR) and median raphe (MR) regions depicted in B and C, respectively (adapted from Paxinos & Franklin, 2001). (B and C) Fluorescent images of GFP-positive neurons and tryptophan hydroxylase (TrypH)-positive (serotonergic) neurons labeled with streptavidin–Cy3 (red). Note that GFP-positive neurons are largely absent from midline areas where TrypH-positive neurons are most highly concentrated. For abbreviations, see legend for Fig. 1. Scale bars: 150 μm.

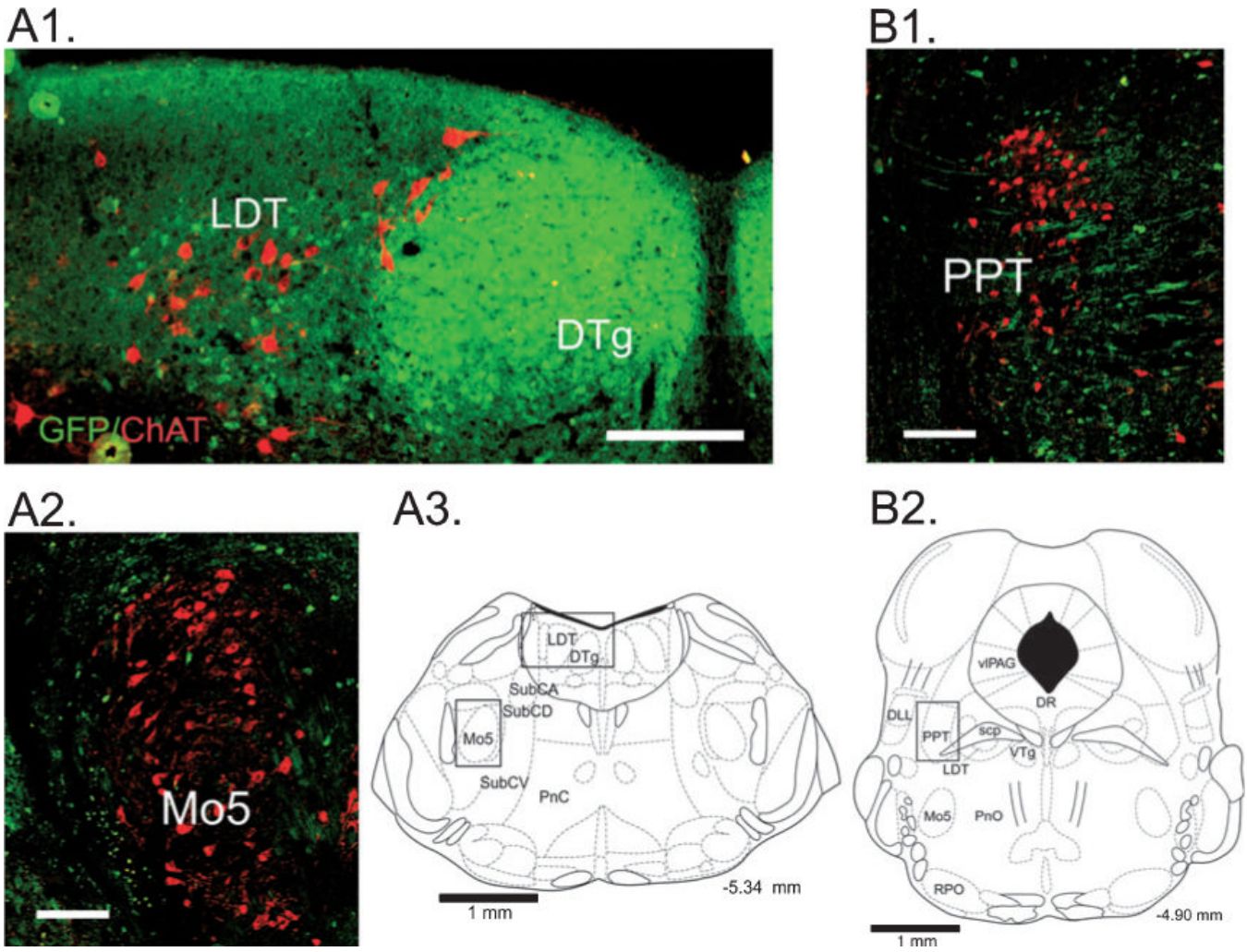

Fig. 3.

Relationship of green fluorescent protein (GFP)-positive neurons to cholinergic brainstem neurons. Fluorescent images of GFP-positive neurons and choline acetyltransferase (ChAT)-positive (cholinergic) neurons labeled with streptavidin–Cy3 (red). (A1) At the level of the caudal laterodorsal tegmental nucleus, numerous small GFP-positive neurons are densely packed in the dorsal tegmental nucleus of Gudden (DTg) and are intermingled with larger ChAT-positive neurons in the laterodorsal tegmentum (LDT). (A2) GFP-positive neurons form a ring around cholinergic motoneurons of the trigeminus (Mo5). (A3) Schematic indicating the locations (rectangles) of the regions depicted in A1 and A2 (adapted from Paxinos & Franklin, 2001). (B1) Small GFP-positive neurons are intermingled with larger ChAT-positive neurons in the pedunculopontine tegmental nucleus (PPT). GFP is also present within fibers in this area. (B2) Schematic indicating the location (rectangle) of the region depicted in B1 (adapted from Paxinos & Franklin, 2001). For abbreviations, see legend for Fig. 1. Scale bars: 150 μm.

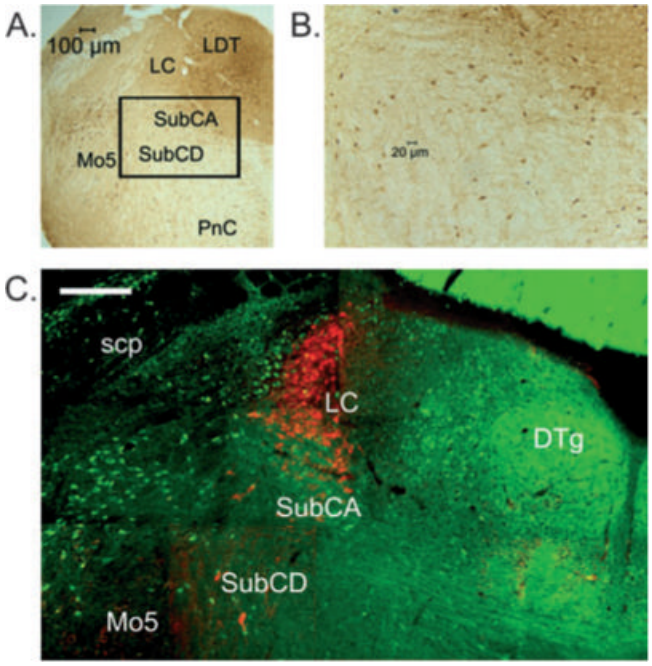

Fig. 4.

Green fluorescent protein (GFP)-positive neurons are located within the subcoeruleus (SubC) area that is important for REM muscle atonia. (A) Location of the SubC area ventral to the locus coeruleus (LC). The slide was processed for anti-GFP staining revealed using diaminobenzidine (DAB). The area indicated by the rectangle is shown at higher power in B. A moderate number of round or triangular-shaped neurons (stained brown) can be seen in this area. (C) Fluorescent image of GFP-positive neurons and tyrosine hydroxylase (TyH)-positive (noradrenaline) neurons labeled with streptavidin–Cy3 (red) at the level of the main part of the LC. GFP-positive neurons are intermingled with scattered larger TyH-positive neurons ventral to the LC in the alpha (SubCA) and dorsal (SubCD) parts of the SubC. For abbreviations, see legend for Fig. 1. Scale bar: 200 µm.

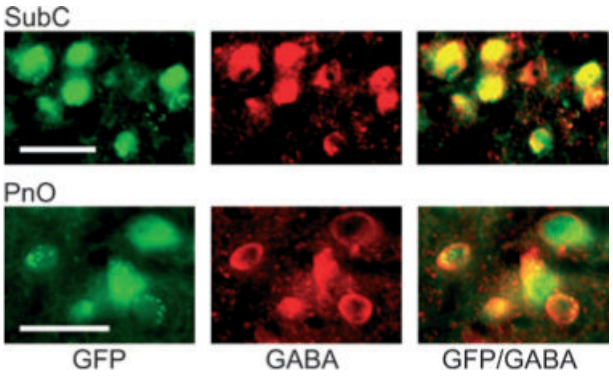

Fig. 5.

Green fluorescent protein (GFP)-positive neurons contain GABA in the subcoeruleus (SubC) and pontine nucleus oralis (PnO) regions used for electrophysiological recordings. Left: Fluorescent images of GFP-positive neurons. Note that the fluorescence fills the entire cell, including the nucleus. Note also that punctate green fluorescence suggestive of axon terminals can be observed over the somata of several neurons (especially in the PnO). Middle: Fluorescent images of neurons stained for GABA/streptavidin–Cy3 (red). Note that the staining is cytoplasmic and avoids the nucleus. Right: Overlay of the green and red fluorescent images reveals that the GFP-positive neurons (green) in the SubC and PnO contain GABA (red), producing an orange color or orange with a green center (GFP in the nucleus). Scale bars: 25 μm.

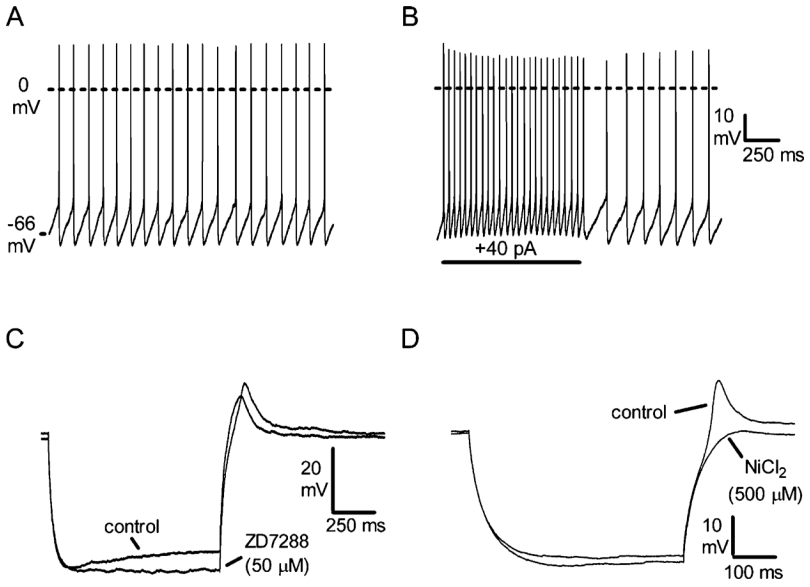

Fig. 6.

Intrinsic membrane properties of subcoeruleus (SubC) and pontine nucleus oralis (PnO) green fluorescent protein (GFP)-positive neurons (n = 61). (A) Spontaneous action potential firing (scale same as in B). (B) Increased tonic firing in response to depolarizing current step. (C) Response to hyperpolarizing current injection (−130 pA) in the presence of tetrodotoxin (TTX, 0.5 μM), illustrating a medium-sized depolarizing sag during the step that is blocked by the H-current blocker ZD7288 (n = 7/7). Note that the rebound depolarization at the offset of the step is slightly increased in size by the block of I_h. (D) Response to a smaller hyperpolarizing current step (−100 pA) in a different neuron, illustrating a rebound depolarization that is blocked by the calcium channel antagonist $NiCl_2$ (n = 9/9).

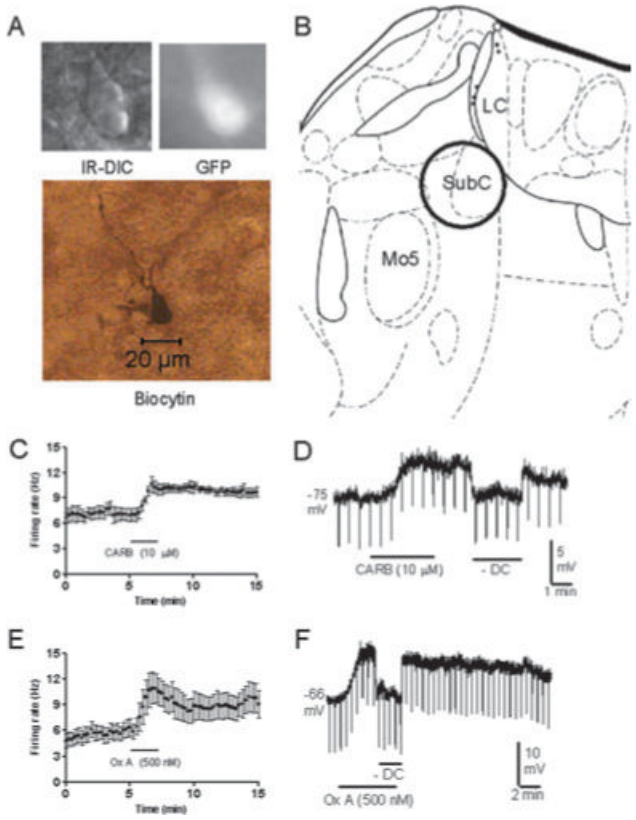

Fig. 7.

Pharmacological properties of green fluorescent protein (GFP)-positive neurons in the subcoeruleus (SubC). (A) Infrared differential interference contrast (IR-DIC) image, black-and-white image of GFP fluorescence, and post hoc biocytin stain (below) of the recorded neuron. (B) Location of the SubC in the mouse brainstem (adapted from Paxinos & Franklin, 2001). LC, locus coeruleus; Mo5, motor trigeminal nucleus. (C and D) Response of neurons to carbachol (CARB) in cell-attached mode (C, $n = 5/5$) and in whole-cell current-clamp mode in the presence of tetrodotoxin (D, $n = 5/5$). SubC GFP-positive neurons were excited by CARB. (E and F) Response of neurons to orexin A (Ox A) in cell-attached mode (E, $n = 7/7$) and in whole-cell current-clamp mode in the presence of tetrodotoxin (F, $n = 5/5$). SubC GFP-positive neurons were excited by Ox A. Downward deflections in D and F reflect hyperpolarizing current pulses used to monitor input resistance. Hyperpolarizing current injection (–DC) was used so as to compare input resistance at the baseline membrane potential.

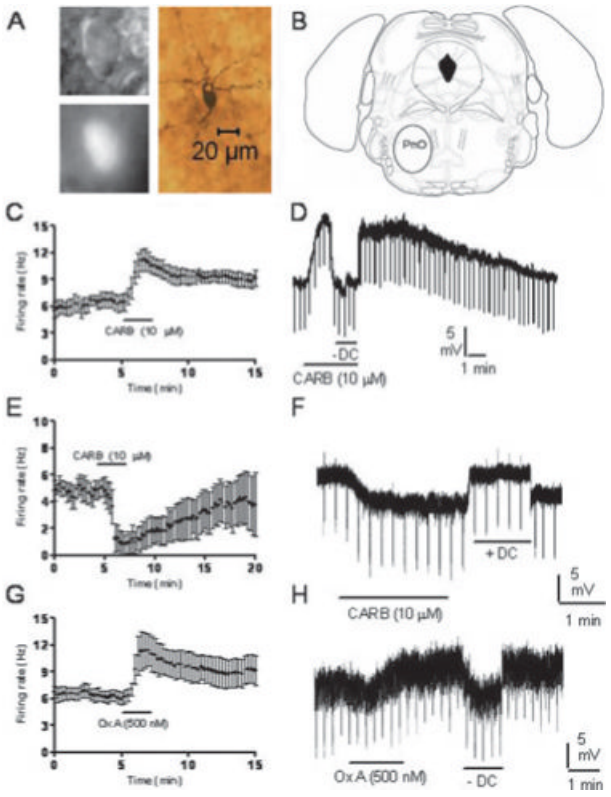

Fig. 8.

Pharmacological properties of green fluorescent protein (GFP)-positive neurons in the pontine nucleus oralis (PnO). (A) Infrared differential interference contrast (IR-DIC) image, black-and-white image of GFP fluorescence, and *post hoc* biocytin stain (below) of the recorded neuron. (B) Location of the PnO in the mouse brainstem (adapted from Paxinos & Franklin, 2001). (C–F) Response of neurons to carbachol (CARB) in cell-attached mode (C and E) or in whole-cell current-clamp mode in the presence of tetrodotoxin (D and F). Different populations of PnO GFP-positive neurons were excited (C and D; $n = 8/12$, $n = 7/11$, respectively) or inhibited (E and F; $n = 4/12$, $n = 4/11$, respectively) by CARB. (E and F) Response of neurons to orexin A (Ox A) in cell-attached mode (G, $n = 6/6$) or in whole-cell current-clamp mode in the presence of tetrodotoxin (H, $n = 9/9$). PnO GFP-positive neurons were excited by Ox A. Downward deflections in D and F reflect hyperpolarizing current pulses used to monitor input resistance. Hyperpolarizing current injection (–DC) was used so as to compare input resistance at the baseline membrane potential. Note that the recording presented in H appears noisy due to a high frequency of spontaneous inhibitory synaptic potentials.